

# Photoacoustic tomography of biological tissues with high cross-section resolution: Reconstruction and experiment

Xueding Wang, Yuan Xu, and Minghua Xu

*Optical Imaging Laboratory, Biomedical Engineering Program, Texas A&M University, 3120 TAMU, College Station, Texas 77843-3120*

Seiichirou Yokoo and Edward S. Fry

*Department of Physics, Texas A&M University, 4242 TAMU, College Station, Texas 77843-4242*

Lihong V. Wang<sup>a)</sup>

*Optical Imaging Laboratory, Biomedical Engineering Program, Texas A&M University, 3120 TAMU, College Station, Texas 77843-3120*

(Received 26 December 2001; accepted for publication 25 September 2002; published 27 November 2002)

A modified back-projection approach deduced from an exact reconstruction solution was applied to our photoacoustic tomography of the optical absorption in biological tissues. Pulses from a Ti:sapphire laser (4.7 ns FWHM at 789.2 nm) were employed to generate a distribution of photoacoustic sources in a sample. The sources were detected by a wide-band nonfocused ultrasonic transducer at different positions around the imaging cross section perpendicular to the axis of the laser irradiation. Reconstructed images of phantoms made from chicken breast tissue agreed well with the structures of the samples. The resolution in the imaging cross section was experimentally demonstrated to be better than 60  $\mu\text{m}$  when a 10 MHz transducer (140% bandwidth at  $-60$  dB) was employed, which was nearly diffraction limited by the detectable photoacoustic waves of the highest frequency. © 2002 American Association of Physicists in Medicine.

[DOI: 10.1118/1.1521720]

Key words: photoacoustic tomography, optoacoustic tomography, laser, reconstruction, imaging

## I. INTRODUCTION

Recently, there has been considerable interest in photoacoustic tomography, a nonionizing imaging modality based upon differential absorption of electromagnetic waves for different tissue types. It is well known that some tissues, such as malignant tumors, melanin-pigmented lesions, and blood vessels have obviously higher absorption rates compared with surrounding tissues. For example, the absorption contrast between breast tumors and normal breast tissues can be as high as 300% for 1064 nm light;<sup>1</sup> the absorption contrast between the blood and the surrounding medium is around 1000% for 850 nm light.<sup>2</sup> The thermal expansion of an absorption structure in tissue creates acoustic waves according to the thermoelastic mechanism, which can be detected by high sensitive piezoelectric devices outside the sample. Photoacoustic tomography visualizes the high optical contrast between different soft biological tissues instead of the low acoustic contrast while retaining the satisfactory spatial resolution of pure ultrasound imaging.

The photoacoustic method to detect small deeply embedded tumors has been studied by Esenaliev *et al.*<sup>3</sup> and Oraevsky *et al.*<sup>4,1</sup> In an attempt to advance the *in vivo* detection of skin cancer, photoacoustic imaging of layered tissues with optical contrast has been studied by Beenen *et al.*,<sup>5</sup> Oraevsky *et al.*,<sup>6</sup> and Karabutov *et al.*<sup>7</sup> Axial resolution up to 10–20  $\mu\text{m}$  has been achieved. Hoelen *et al.* applied photoacoustic tomography to the detection of blood concentrations.<sup>2</sup> The depth resolution of blood vessel imaging in highly scattering media is about 10  $\mu\text{m}$ . Paltauf *et al.* adopted an optical

method instead of piezoelectric devices for two-dimensional (2D) ultrasonic detection and achieved a spatial resolution around 10  $\mu\text{m}$ .<sup>8</sup>

All of the above photoacoustic tomography systems can be categorized into two detection modes: (1) the forward mode, with the laser irradiation and ultrasound detection on opposite surfaces of the sample, and (2) the backward mode, with the laser irradiation and ultrasound detection on the same surface of the sample. Although high resolution along the axis of the laser irradiation can be easily achieved, the basic problem with these two modes is the poor lateral resolution, which is limited mainly by the scanning range of the detector.

When lateral resolution is the concern or the imaging purpose is to obtain a 2D image of a cross section of the sample perpendicular to the axis of the laser irradiation, a proper scheme is to arrange the receiver around the laser axis to detect the acoustic signals from the side of the sample. A focused ultrasonic transducer can be adopted to perform the linear, or sector, scan, and then the measured data is used to construct an image directly,<sup>9</sup> which is similar to the method used in early pulse-echo ultrasonography. An alternative method is to use a wide-band point detector to receive the acoustic signals and then reconstruct the absorption distribution based on a certain algorithm.<sup>10,11</sup>

On the other hand, when employing the nonfocused ultrasonic transducer for detection, the quality of the photoacoustic imaging is highly dependent on the reconstruction algorithm. Examples of approximate reconstruction algorithms

include the weighted delay-and-sum method,<sup>12</sup> the optimal statistical approach,<sup>13</sup> and the Radon transform in far-field approximation.<sup>10,14,15</sup> Exact reconstruction algorithms were recently derived for various detection geometries.<sup>16-19</sup>

In this paper, a modified back-projection method based on the circular-scan geometry was applied to the photoacoustic tomography of optical absorption in biological tissues. The modified back-projection algorithm was deduced from an exact reconstruction solution in the time domain, which will be briefly introduced in the second section. In the third section, the experimental method, as well as the imaging results in tissue phantoms, will be shown. In the fourth section, the best resolution in the cross section of our photoacoustic tomography system will be demonstrated by experimental results. The final section will present our conclusions.

## II. MODIFIED BACK-PROJECTION

We are interested in tissues with inhomogeneous optical absorption but relatively homogeneous acoustic properties. When the laser pulse is very short, which is the case in our experiments, the time required for thermal diffusion is much greater than the time for the thermoacoustic transition. Consequently, the effect of heat conduction in the thermoacoustic wave equations can be ignored. As has been described previously in the literatures,<sup>20,21</sup> the generation of a photoacoustic wave by deposition of light energy can be expressed as

$$\frac{\partial^2 p(\mathbf{r}, t)}{\partial t^2} - v_s^2 \nabla^2 p(\mathbf{r}, t) = \frac{v_s^2 \beta}{C_p} \frac{\partial H(\mathbf{r}, t)}{\partial t}, \quad (1)$$

where  $v_s$  is the acoustic speed;  $C_p$  is the specific heat;  $\beta$  is the thermal coefficient of volume expansion; and  $H(\mathbf{r}, t)$  is the heat-producing radiation deposited in the tissue per unit volume per unit time, which can be expressed as

$$H(\mathbf{r}, t) = \varphi(\mathbf{r}) \eta(t), \quad (2)$$

where  $\varphi(\mathbf{r})$  describes the optical energy deposition (also called optical absorption) within the tissue at position  $\mathbf{r}$ ;  $\eta(t)$  describes the shape of the irradiation pulse, which can be further expressed as  $\eta(t) = \delta(t)$  for delta-function laser pulses.

The object of the image reconstruction is to estimate the distribution of the optical absorption  $\varphi(\mathbf{r})$  of the tissue from a set of measured acoustic signals  $p(\mathbf{r}, t)$ . For a circular scanning configuration, the exact inverse solution can be derived based on the spherical harmonic function,

$$\begin{aligned} \varphi(\mathbf{r}) = & \frac{1}{4 \pi^2 \lambda v_s r_0^2} \int_{S_0} \int dS_0 \int_{-\infty}^{+\infty} dk \bar{p}(\mathbf{r}_0, k) \\ & \times \sum_{m=0}^{\infty} \frac{(2m+1) j_m(kr)}{h_m^{(1)}(kr_0)} P_m(\mathbf{n} \cdot \mathbf{n}_0), \end{aligned} \quad (3)$$

where  $\lambda = \beta/C_p$ ;  $\mathbf{n} = \mathbf{r}/r$ ;  $\mathbf{n}_0 = \mathbf{r}_0/r_0$ ;  $\mathbf{r}_0$  is the detector position in respect to the imaging center;  $k = \omega/v_s$  is the wave number;  $\bar{p}(\mathbf{r}_0, k)$  is the Fourier transform of the pressure function  $p(\mathbf{r}_0, t)$ ;  $S_0$  is the measurement surface including

the object under investigation;  $j_l(\cdot)$  and  $h_l^{(1)}(\cdot)$  are the spherical Bessel and Hankel functions, respectively; and  $P_l(\cdot)$  represents the Legendre polynomial. The detailed derivation of this exact inverse solution can be found elsewhere.

This inverse solution involves a summation of a series that is computationally time consuming. Therefore, it is desirable to simplify the solution. In the experiments, the detection radius  $r_0$  is much larger than the wavelengths of the photoacoustic waves that are used for imaging. Therefore, we can assume  $|k|r_0 \gg 1$  and use the asymptotic form of the Hankel function to simplify the above exact inverse solution Eq. (3). The approximate inverse solution has the form of

$$\varphi(\mathbf{r}) = - \frac{1}{2 \pi v_s^4 \lambda} \int_{S_0} \int dS_0 \frac{1}{t} \frac{\partial p(\mathbf{r}_0, t)}{\partial t} \Big|_{t=|\mathbf{r}_0-\mathbf{r}|/v_s}. \quad (4)$$

Actually, two compensation factors are implicit in this solution. Firstly, we introduce a weighting factor “ $t$ ,” which compensates for the  $1/t$  attenuation of a spherical pressure wave as it propagates through a homogeneous medium. At the same time, we consider that in this type of reconstruction geometry, the contribution to a certain point  $P$  from an element of receiving area  $S$  is proportional to the subtended solid angle of this element  $S$  when viewed from the point  $P$ . The solid angle is inversely proportional to the square of the distance between the receiving element  $S$  and the point  $P$ , which leads to a compensation factor of “ $1/t^2$ .” Combining the above two factors, we obtain a compensation factor of “ $1/t$ ” as shown in Eq. (4).

Reference 15 gave an approximate solution of  $\varphi(\mathbf{r})$  based on a three-dimensional inverse Radon transformation with the assumption that the size of an absorption object is much less than the distance between the source and the detector. In that case, the spherical surface over which the surface integral is computed approximates a plane. Actually, with the above assumption,  $t$  is nearly a constant compared to the size of the absorption object. However, in most cases, for example, the situation in our experiments, the size of an absorption object can be comparable to the distance between the source and the detector. Under this condition, the solution given by Ref. 15 is not appropriate, while our solution shown in Eq. (4) still holds and therefore is more general.

Although the modified back-projection reconstruction shown in Eq. (4) is valid for three-dimensional distributions of photoacoustic sources, we here consider only the imaging of thin slices of absorption objects in turbid media to evaluate our imaging system. The slices of absorption objects lie in the imaging plane perpendicular to the axis of laser irradiation. The photoacoustic signals from turbid media outside the imaging plane are regarded as background that will not provide information for the imaging of absorption objects. In this case, the detection of acoustic pressures over the  $2\pi$  angle in the imaging plane is sufficient to achieve high resolution in the imaged cross section. For 2D imaging, the approximate inverse solution for the circular-scan geometry can be represented by

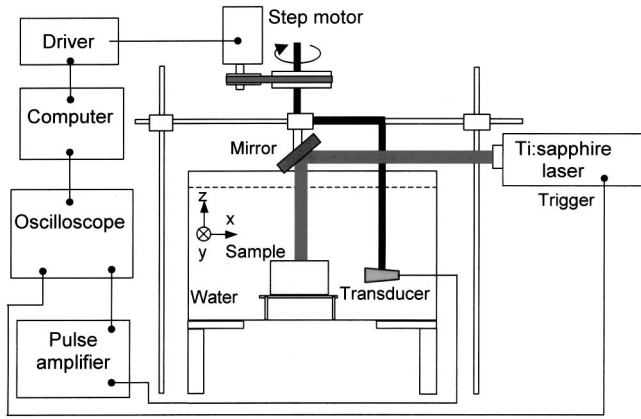


FIG. 1. Experimental setup.

$$\varphi(\mathbf{r}) = -\frac{r_0^2}{2\pi\lambda v_s^4} \int_{\theta_0} d\theta_0 \frac{1}{t} \frac{\partial p(\mathbf{r}_0, t)}{\partial t} \Big|_{t=|\mathbf{r}_0-\mathbf{r}|/v_s}, \quad (5)$$

which is an integral over  $\theta_0$  around the thin slice of the object. From Eqs. (4) and (5), we see that the reconstruction of the absorption distribution can be fulfilled by back-projection of the quantity

$$-\frac{1}{t} \frac{\partial p(r_0, t)}{\partial t} \Big|_{t=|\mathbf{r}_0-\mathbf{r}|/v_s}$$

instead of the acoustic pressure  $p(\mathbf{r}_0, t)$ .

If  $R(t)$  is the impulse response of the detector and  $P(t)$  is the pulse duration of the laser, in the time domain, we have

$$T(\mathbf{r}_0, t) = p(\mathbf{r}_0, t) * R(t) * P(t), \quad (6)$$

where  $T(\mathbf{r}_0, t)$  is the piezoelectric signal detected by the transducer, and  $*$  represents convolution. Then,  $\partial p(\mathbf{r}_0, t)/\partial t$  in Eq. (5) can be calculated by an inverse Fourier transformation,

$$\begin{aligned} \frac{\partial p(\mathbf{r}_0, t)}{\partial t} &= \text{FFT}^{-1} \left[ \frac{-i\omega T(\mathbf{r}_0, \omega) W(\omega)}{P(\omega)R(\omega)} \right] \\ &= \frac{1}{2\pi} \int_{-\infty}^{+\infty} \frac{-i\omega T(\mathbf{r}_0, \omega) W(\omega)}{P(\omega)R(\omega)} \exp(-i\omega t) dt, \quad (7) \end{aligned}$$

where  $W(\omega)$  is a band-pass window function that suppresses the frequency component outside the detectable spectrum of the transducer.

### III. TOMOGRAPHY IN BIOLOGICAL TISSUES

#### A. Experimental method

A schematic diagram of our experimental setup for photoacoustic tomography is shown in Fig. 1, where a laboratory coordinate system  $[x, y, z]$  is also depicted. A flash-lamp-pumped Ti:sapphire laser operating at a wavelength of 789.2 nm with a pulse energy of approximately 30 mJ, a pulse duration of 4.7 ns FWHM, and a repetition rate of 10 Hz, was used as the light source. The laser is expanded to a 1.5 cm diameter beam when heating the sample surface from above along the laser axis; this provides an incident power density within the limit of safety for human skin (100 mJ/cm<sup>2</sup>) according to the ANSI standard.<sup>22</sup> In our experiments, the area in a cross section of the sample that is imaged is defined by the size of the laser beam. The wave form and the frequency spectrum of the laser pulse are demonstrated in Figs. 2(a) and 2(b), respectively, where the curve in (b) shows the component of  $R(\omega)$  in Eq. (7).

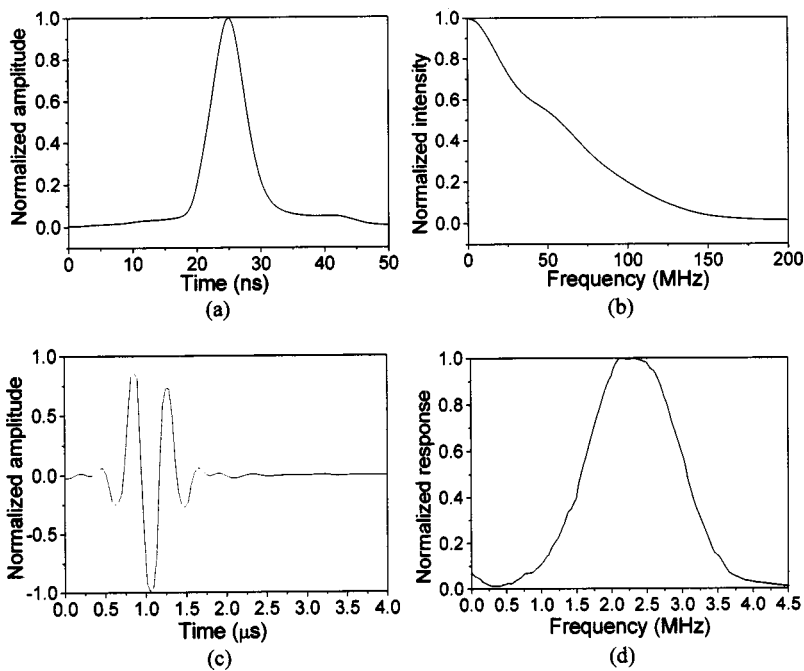


FIG. 2. (a) Wave form and (b) frequency spectrum of the 4.7 ns laser pulse. (c) Impulse response and (d) frequency response of the 2.25 MHz transducer.

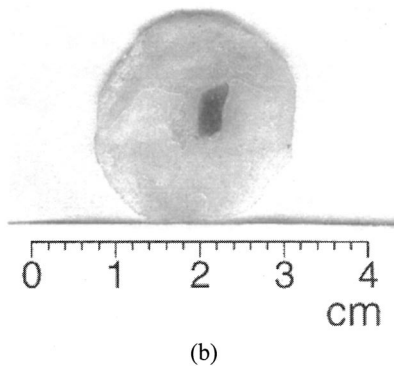
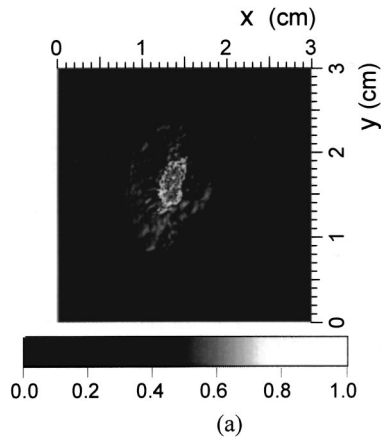


FIG. 3. Photoacoustic tomography of a slice of chicken gizzard that was buried 0.5 cm deep in the chicken breast slab. (a) Reconstructed image; (b) picture of the imaged cross-section of the sample.

The wide-band nonfocused transducer (V323, Panametrics) has a 2.25 MHz central frequency and a 6 mm diameter of the active element. The impulse response and the frequency response of the transducer are demonstrated in Figs. 2(c) and 2(d), respectively, where the curve in Fig. 2(d) shows the component of  $P(\omega)$  in Eq. (7). Because the frequency bandwidth of the laser pulse is much broader than that of the transducer,  $P(\omega)$  is constant and Eq. (7) can be simplified as

$$\frac{\partial p(\mathbf{r}_0, t)}{\partial t} \propto \frac{1}{2\pi} \int_{-\infty}^{+\infty} \frac{-i\omega T(\mathbf{r}_0, \omega) W(\omega)}{R(\omega)} \exp(-i\omega t) dt. \quad (8)$$

The transducer was mounted on a rotation stage that was driven by a computer-controlled step motor. The transducer scanned around the sample with a rotational step size of  $1.125^\circ$  and a rotational radius of 5 cm. The transducer and the sample were immersed in water. A low-noise pulse pre-amplifier (500 PR, Panametrics) amplified the acoustic signals received by the transducer and sent signals to an oscilloscope (TDS-640A, Tektronix). Then, 30 times averaged digital signals were transferred to a computer for imaging.

The experiments were performed with thin slices of gizzard tissues or red rubber pieces placed 0.5 cm deep in fresh chicken breast muscle slabs. For 789.2 nm light the reduced scattering coefficient  $\mu'_s$  and the absorption coefficient  $\mu_a$  for chicken breast tissue are about  $1.9 \text{ cm}^{-1}$  and  $0.1 \text{ cm}^{-1}$ , respectively.<sup>23</sup> Under this condition, the effective optical at-

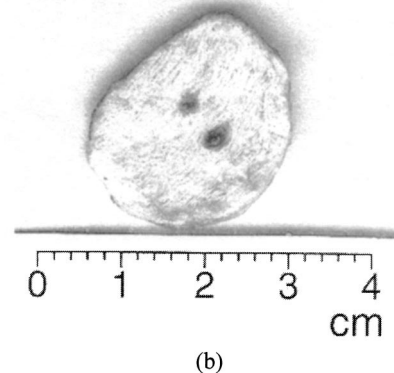
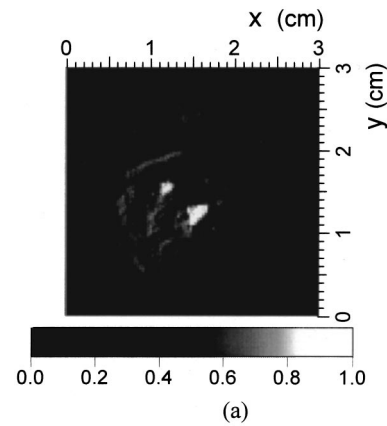


FIG. 4. Photoacoustic tomography of two slices of chicken gizzard that were buried 0.5 cm deep in the chicken breast slab. (a) Reconstructed image; (b) picture of the imaged cross-section of the sample.

tenuation coefficient  $\mu_{\text{eff}}$  is  $0.77 \text{ cm}^{-1}$ . The blood concentration in the chicken gizzard tissue is much higher than that in the chicken breast muscle. According to our measurements, the absorption contrast between them is greater than 200%. In the experiments, the sizes of the chicken breast slabs were larger than the size of the laser beam. Therefore, the imaged area is only a part of a cross section of the sample.

## B. Imaging results

Image reconstruction utilized the 2D modified back-projection algorithm described in Eq. (5). We used  $1.5 \text{ mm}/\mu\text{s}$  as the estimated sound velocity  $\nu_s$  in soft tissues. When a detected sample has nearly homogeneous acoustic properties, the small difference between the actual sound velocity and the estimated value will not cause any distortion in the relative location of the absorption distribution in the sample. In other words, the absolute locations and sizes of the detected targets inside the sample may be changed; however, their relative positions will not be altered.

Figure 3(a) shows the reconstructed image of a thin slice of gizzard tissue buried 0.5 cm deep in a chicken breast slab. The gizzard tissue has a nearly rectangular shape (3 mm  $\times$  6 mm) in the imaging plane and a thickness of about 1 mm. The picture of the cross section of this sample is shown in Fig. 3(b) for comparison. In the second sample, two slices of

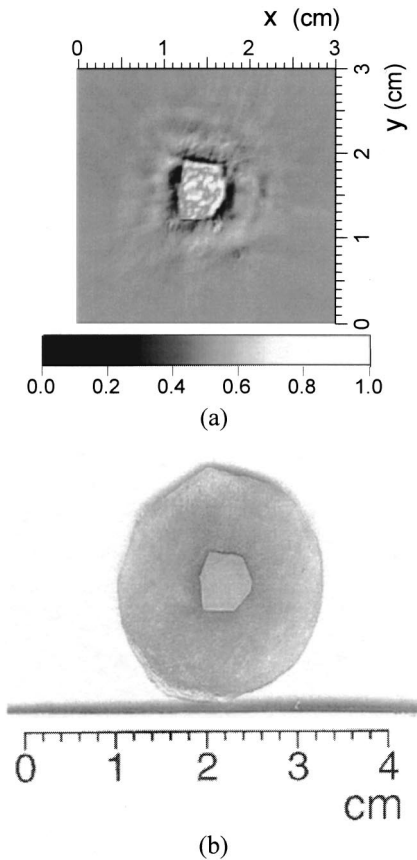


FIG. 5. Photoacoustic tomography of a slice of rubber that was buried 0.5 cm deep in the chicken breast slab. (a) Reconstructed image; (b) picture of the imaged cross-section of the sample.

gizzard tissues are placed 0.5 cm deep in a chicken breast slab, where the sizes of the two gizzard pieces are different. The reconstructed imaging is shown in Fig. 4(a) for comparison with the picture of the sample in Fig. 4(b).

Based on our experimental system as well as the reconstruction algorithm, the results of the 2D photoacoustic tomography are satisfying. The highly absorbing objects in turbid media with comparatively low absorption were localized well. The boundaries between the gizzards and the chicken breast are clearly imaged.

Because both the gizzards and the chicken breast muscles are soft biological tissues, it is difficult to avoid deformation when the samples were photographed. For this reason, the shapes of the gizzard slices in the reconstructed imaging have minor discrepancies with those appearing in the photographs. To overcome this problem, slices of red rubber pieces were used as absorption objects in some of our experiments. Figure 5(a) shows the reconstructed image of a slice of rubber (with a 1 mm thickness) that was buried 0.5 cm deep in a chicken breast slab; it fits perfectly with the picture of the sample shown in Fig. 5(b). In another sample, three circles of rubber slices with a 1 mm thickness, where the radii of the three circles are about 4 mm, 3 mm, and 1 mm, respectively, were adopted as absorption objects. In Figure 6(a), the shapes and sizes as well as the localizations of the three rubber slices are all imaged well compared with the picture

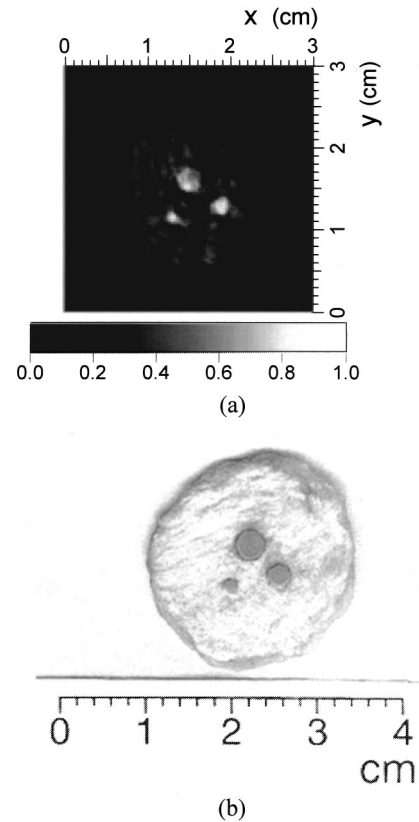


FIG. 6. Photoacoustic tomography of three slices of rubber circles that were buried 0.5 cm deep in the chicken breast slab. The radii of the three circles are 0.4 cm, 0.3 cm, and 0.1 cm, respectively. (a) Reconstructed image; (b) picture of the imaged cross-section of the sample.

in Fig. 6(b). In the reconstructed images in Figs. 3–6, we can see some intensity fluctuations around the absorption objects, which come mainly from the photoacoustic signals generated in the background chicken breast tissues.

#### IV. TESTING FOR RESOLUTION

In order to quantify the actual resolution of our detection system as well as the reconstruction algorithm, well-controlled samples with high absorption contrast in transparent media were measured for imaging. Usually, the expected highest spatial resolution is estimated to be the half wavelength at the center frequency of the transducer. However, when the frequencies of the detected photoacoustic signals determining the spatial resolution are higher than the center frequency, the achievable spatial resolution is better than the estimated resolution at the center frequency. Therefore, we estimate the possible best resolution to be the half wavelength at the highest detectable photoacoustic frequency.

Pairs of parallel lines printed on transparencies were adopted as ideal testing samples, as shown in Fig. 7(a). The length and width of the dark lines was 8 mm and 0.3 mm, respectively. The gap  $d$  between the two lines was set to be 0.1 mm, 0.2 mm, and 0.3 mm, respectively. Each piece of transparency with a pair of dark lines was placed in the imaging plane. The 2.25 MHz nonfocused transducer scanned-

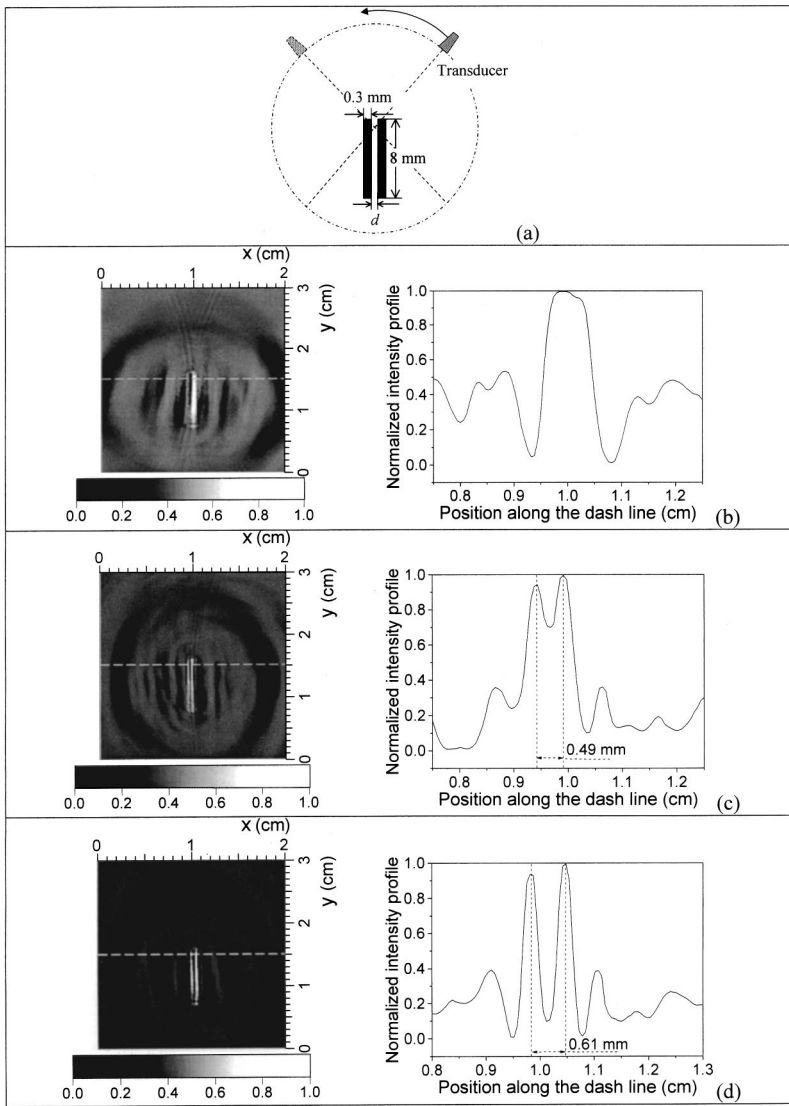


FIG. 7. (a) Schematic of a pair of parallel lines printed on transparency. The length of the two lines is 8 mm; the width of the two lines is 0.3 mm; and the gap between the two lines was  $d$ . The radius of the circular-scan is 50 mm. (b), (c), and (d) are the reconstructed images of the pairs of parallel lines with a gap  $d$  of 0.1 mm, 0.2 mm, and 0.3 mm, respectively. The profiles of reconstructed absorption intensities along the dash lines in 2D images are demonstrated as the right pictures in (b), (c), and (d), respectively.

around the transparency with a radius of 5 cm. The detectable frequency band of the transducer is from 0 to 4.5 MHz. Therefore, the estimated highest spatial resolution is 0.17 mm. The reconstructed 2D images of these pairs of lines are

shown in Figs. 7(b), 7(c), and 7(d) for  $d$  equals 0.1 mm, 0.2 mm, and 0.3 mm, respectively. The intensity profiles along the dashed lines ( $y=1.5$  cm) in the 2D images are also presented. When  $d$  equals 0.2 mm or 0.3 mm, the two parallel lines can be recognized with an obvious gap between them. However, when  $d$  equals 0.1 mm, we can see only one line in the reconstructed image. In each image, there are some weak intensity fluctuations around the pair of lines, which come mainly from acoustic reflection at the edge of the transparency piece. The results in Fig. 7 show that with the circular-scan method and the modified back-projection algorithm, we can achieve a spatial resolution of  $\sim 0.2$  mm.

The center of the circular scan in the experiments is taken at the center of each reconstructed image. We can see that in these 2D images, the spatial resolution at a position near the imaging center is higher than that at a longer distance from the imaging center. This kind of blur in the reconstructed image is mainly caused by the physical size of the transducer. The blur is greater when the physical size of the transducer is larger, or the distance from the imaging center is larger.

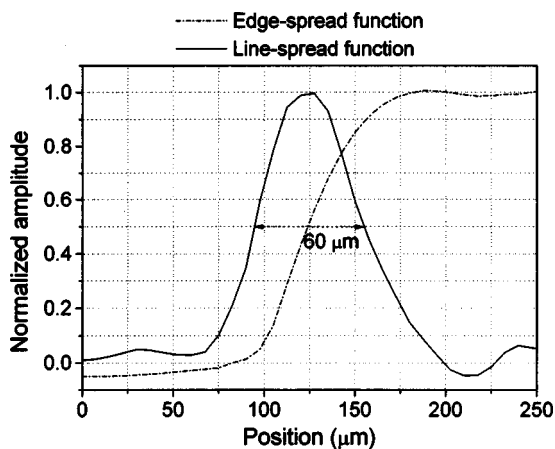


FIG. 8. Edge-spread function and line-spread function of our photoacoustic imaging system with a 10 MHz transducer.

We quantified the spatial resolution of our imaging system with a 10 MHz wide-band (140% at  $-60$  dB) cylindrically focused transducer (V312, Panametrics). The transducer has a 6 mm diameter active element and is nonfocused in the imaging plane. The estimated highest spatial resolution of our imaging system with this transducer is about  $45 \mu\text{m}$ . A well-controlled phantom made from red rubber with a high optical absorption contrast and a sharp edge has been imaged to obtain the edge-spread function. A line-spread function was obtained through differentiating the profile of the edge-spread function. Both the two profiles are shown in Fig. 8. The line-spread function shows a full width at half maximum of about  $60 \mu\text{m}$ , which shows that the spatial resolution of our photoacoustic imaging system is near the diffraction limit of the detected photoacoustic signals.

## V. CONCLUSION

Pulsed-laser induced photoacoustic tomography of absorption in biological tissues has been studied. A modified back-projection algorithm derived from an exact inverse solution was used to reconstruct the signals received by a wide-band nonfocused transducer that scanned circularly around the sample under detection. Reconstructed images of gizzard slices and rubber slices buried in chicken breast tissues agree well with the pictures of samples. Experiments also quantified the highest 2D resolution that can be achieved by this imaging system: using a detection of  $2\pi$  view, the spatial resolution is nearly diffraction limited by the detected photoacoustic waves.

Our photoacoustic detection system with the modified back-projection reconstruction algorithm is proved to be an effective method for biological tissue imaging with high contrast and high spatial resolution. If a high resolution along the laser axis is required at the same time, scanning of acoustic signals along the axis will be necessary.

## ACKNOWLEDGMENTS

This project was sponsored in part by the U.S. Army Medical Research and Materiel Command Grant No. DAMD 17-00-1-0455, the National Institutes of Health Grant No. R01 CA71980, the National Science Foundation Grant No. BES-9734491, Texas Higher Education Coordinating Board Grant No. ARP 000512-0123-1999, and the Robert A. Welch Foundation Grant No. A-1218.

<sup>a)</sup> Author to whom correspondence should be addressed. Electronic mail: lwang@tamu.edu (URL: <http://oilab.tamu.edu>).

<sup>1</sup> A. A. Oraevsky, V. A. Andreev, A. A. Karabutov, D. R. Fleming, Z. Gatalica, H. Singh, and R. O. Esenaliev, "Laser opto-acoustic imaging of the breast: detection of cancer angiogenesis," *Proc. SPIE* **3597**, 352–363 (1999).

- <sup>2</sup> C. G. A. Hoelen, F. F. M. de Mul, R. Pongers, and A. Dekker, "Three-dimensional photoacoustic imaging of blood vessels in tissue," *Opt. Lett.* **23**, 648–650 (1998).
- <sup>3</sup> R. O. Esenaliev, A. A. Karabutov, and A. A. Oraevsky, "Sensitivity of laser opto-acoustic imaging in detection of small deeply embedded tumors," *IEEE J. Sel. Top. Quantum Electron.* **5**, 981–988 (1999).
- <sup>4</sup> R. O. Esenaliev, F. K. Tittel, S. L. Thomsen, B. Fornage, C. Stelling, A. A. Karabutov, and A. A. Oraevsky, "Laser optoacoustic imaging for breast cancer diagnostics: Limit of detection and comparison with x-ray and ultrasound imaging," *Proc. SPIE* **2979**, 71–82 (1997).
- <sup>5</sup> A. Beenen, G. Spanner, and R. Niessner, "Photoacoustic depth-resolved analysis of tissue models," *Appl. Spectrosc.* **51**, 51–57 (1997).
- <sup>6</sup> A. A. Oraevsky, R. O. Esenaliev, and A. Karabutov, "Laser optoacoustic tomography of layered tissues: Signal processing," *Proc. SPIE* **2979**, 59–70 (1997).
- <sup>7</sup> A. A. Karabutov, E. V. Savateeva, and A. A. Oraevsky, "Imaging of layered structures in biological tissues with opto-acoustic front surface transducer," *Proc. SPIE* **3601**, 284–295 (1999).
- <sup>8</sup> G. Paltauf and H. Schmidt-Kloiber, "Optical method for two-dimensional ultrasonic detection," *Appl. Phys. Lett.* **75**, 1048–1050 (1999).
- <sup>9</sup> M. H. Xu, G. Ku, and L. V. Wang, "Microwave-induced thermoacoustic tomography using multi-sector scanning," *Med. Phys.* **28**, 1958–1963 (2001).
- <sup>10</sup> R. A. Kruger, P. Liu, Y. R. Fang, and C. R. Appledorn, "Photoacoustic ultrasound (PAUS)–Reconstruction tomography," *Med. Phys.* **22**, 1605–1609 (1995).
- <sup>11</sup> A. M. Reyman, I. V. Yahovlev, A. G. Kirillov, and V. V. Lozhkarev, "Deep tomography of biological tissues by optoacoustic method," *Proc. SPIE* **4256**, 159–166 (2001).
- <sup>12</sup> C. G. A. Hoelen and de F. F. M. Mul, "Image reconstruction for photoacoustic scanning of tissue structures," *Appl. Opt.* **39**, 5872–5883 (2000).
- <sup>13</sup> Y. V. Zhulina, "Optimal statistical approach to optoacoustic image reconstruction," *Appl. Opt.* **39**, 5971–5977 (2000).
- <sup>14</sup> R. A. Kruger, D. R. Reinecke, and G. A. Kruger, "Thermoacoustic computed tomography—technical considerations," *Med. Phys.* **26**, 1832–1837 (1999).
- <sup>15</sup> R. A. Kruger, W. L. Kiser, K. D. Miller, H. E. Reynolds, D. R. Reinecke, G. A. Kruger, and P. J. Hofacker, "Thermoacoustic CT: imaging principles," *Proc. SPIE* **3916**, 150–159 (2000).
- <sup>16</sup> K. Kostli, M. Frenz, H. Bebie, and H. Weber, "Temporal backward projection of optoacoustic pressure transients using Fourier transform methods," *Phys. Med. Biol.* **46**, 1863–1872 (2001).
- <sup>17</sup> M. Xu and L. V. Wang, "Time-domain reconstruction for thermoacoustic tomography in a spherical geometry," *IEEE Trans. Med. Imaging* **21**, 814–822 (2002).
- <sup>18</sup> Y. Xu, D. Feng, and L. V. Wang, "Exact frequency-domain reconstruction for thermoacoustic tomography: I. Planar geometry," *IEEE Trans. Med. Imaging* **21**, 823–828 (2002).
- <sup>19</sup> Y. Xu, M. Xu, and L. V. Wang, "Exact frequency-domain reconstruction for thermoacoustic tomography: II. Cylindrical geometry," *IEEE Trans. Med. Imaging* **21**, 829–833 (2002).
- <sup>20</sup> G. J. Diebold, T. Sun, and M. I. Khan, "Photoacoustic waveforms generated by fluid bodies," in *Photoacoustic and Photothermal Phenomena III*, edited by D. Bicanic (Springer-Verlag, Berlin, Heidelberg, 1992), pp. 263–269.
- <sup>21</sup> V. E. Gusev and A. A. Karabutov, *Laser Optoacoustics* (American Institute of Physics, New York, 1993).
- <sup>22</sup> American National Standards Institute, American national standard for the safe use of lasers. Standard Z136.1-2000 (ANSI, Inc., New York, NY, 2000).
- <sup>23</sup> G. Marquez, L. V. Wang, S. P. Lin, J. A. Schwartz, and S. L. Thomsen, "Anisotropy in the absorption and scattering spectra of chicken breast tissue," *Appl. Opt.* **37**, 798–804 (1998).